


Anatomy of spin-wave-driven magnetic texture motion via magnonic torques

Hanxu Ai (艾寒旭) and Jin Lan (兰金)^{*}

*Center for Joint Quantum Studies and Department of Physics, School of Science, Tianjin University, Tianjin 300354, China
and Tianjin Key Laboratory of Low Dimensional Materials Physics and Preparing Technology, Tianjin University, Tianjin 300354, China*



(Received 23 November 2022; revised 29 January 2023; accepted 14 February 2023; published 28 February 2023)

The interplay between spin waves and magnetic texture represents the information exchange between the fast and slow dynamical parts of magnetic systems. Here we formulate a set of magnonic torques acting on background magnetic texture, by extracting time-invariant information from the fast precessing spin waves. Under the frame of magnonic torques, we use theoretical formulations and micromagnetic simulations to investigate the spin-wave-driven domain wall motion in two typical symmetry-breaking situations: the rotational symmetry broken by the Dzyaloshinskii-Moriya interaction and the translational symmetry broken by magnetic damping. The torque-based microscopic analyses provide compact yet quantitative tools to reinterpret the magnetic texture dynamics induced by spin waves, beyond the conventional framework of global momentum conservation.

DOI: [10.1103/PhysRevB.107.054441](https://doi.org/10.1103/PhysRevB.107.054441)

I. INTRODUCTION

The spin wave, the propagating disturbance of ordered magnetizations, is one of the basic excitations in magnetic systems. As an alternative angular momentum carrier besides the spin-polarized conduction electron [1], the spin wave possesses advantages of high energy efficiency, the ability to propagate in magnetic insulators [1–3], and integrability with current magnetic storage techniques [4]. With the above merits and rapidly developing experimental techniques [5,6], spin waves are of growing interest from both theoretical and experimental sides [7,8].

Due to intrinsic nonlinearity of various magnetic interactions, the propagation of spin waves is expected to induce rich dynamics of underlying magnetic texture. Using spin waves to harness the magnetic texture, as well as the converse manipulation of spin waves via magnetic texture, offer an integrated scheme toward constructing purely magnetic computing devices [9,10]. Despite the urgent demand, transparent understandings of spin-wave-driving scenarios are impeded by the complexities brought by the fast precession of spin waves, as well as the nonuniform magnetization distribution of magnetic texture. To overcome this obstacle, a powerful approach is exploiting momentum conservation laws that focus on global momentum transfer of linear momentum [11–13], spin angular momentum [14–16], and orbital angular momentum [17–19], as well as their combinations [20–23]. However, requirements of symmetry-preservation impose stringent limitations on the range of applicability of the above momentum transfer scenarios to realistic magnetic systems.

To escape the symmetry limitations and gain more insights into the actions of spin waves, theories focusing on the interaction details are called for, where a useful strategy is to

make the interaction simple in either space or time. Spatially local interaction can be realized by constructing a spin wave packet, and transforming the spin wave packet and magnetic texture into two particle-like objects [24–27]. On the other hand, time invariant interaction can be realized by extracting the magnonic torques from the spin wave, and discarding irrelevant information in fast oscillations. The magnonic torques, although frequently in an incomplete form, have been derived and employed to explore specific magnetic dynamics in several studies [28–31]. Nevertheless, insufficient cross-checking with micromagnetic simulations and the lack of explicit connections with other theoretical models, especially with the conventional momentum transfer models, hinder the full application of the magnonic torques or their variants.

In this work, we systematically recast actions of spin waves on magnetic texture to a full set of magnonic torques, and further establish the generalized Thiele equation for magnetic texture dynamics via these torques. To demonstrate the applicability of these microscopic torques, we investigate the spin-wave-driven domain wall motion in the presence of Dzyaloshinskii-Moriya interaction (DMI) and magnetic damping, for which both rotational and translational symmetries are broken. By capturing the domain wall dynamics in such a typical symmetry-breaking system in the frame of magnonic torques, we partition the overall contribution into multiple aspects of spin waves. The detailed analyses enabled by magnonic torques offer insights in developing purely magnetic information processing technologies.

The rest of paper is organized as follows. In Sec. II, we systematically derive magnonic torques from fast oscillating spin waves, and then formulate a generalized Thiele equation to describe the magnetic texture dynamics induced by these magnonic torques. With the aid of these magnonic torques, a hierarchy for various magnonic driving models is also proposed. Using the simplified scenarios based on magnonic torques, the spin-wave-driven domain wall motion

^{*}Corresponding author: lanjin@tju.edu.cn

in the presence of DMI and magnetic damping, as two typical situations of broken symmetry, are then thoroughly investigated in Sec. III. Comparisons between actions mediated by magnons and electrons, as well as a short conclusion, are given in Sec. IV.

II. MAGNONIC TORQUES AND GENERALIZED THIELE EQUATION

A. Basic model

Consider a magnetic system with its magnetization direction denoted by a unit vector \mathbf{m} ; then the magnetic dynamics is governed by the Landau-Lifshitz-Gilbert (LLG) equation

$$\dot{\mathbf{m}} = -\gamma \mathbf{m} \times \mathbf{h} + \alpha \mathbf{m} \times \dot{\mathbf{m}}, \quad (1)$$

where $\dot{\mathbf{m}} \equiv \partial_t \mathbf{m}$, γ is the gyromagnetic constant, and α is the Gilbert damping constant. Here $\mathbf{h} = -(1/\mu_0 M_s) \delta U / \delta \mathbf{m}$ is the effective magnetic field acting on the magnetization \mathbf{m} , where μ_0 is the vacuum permeability, M_s is the saturation magnetization, and $U = \int u dV$ is the magnetic energy with V the magnetic volume. The magnetic energy density u takes a typical form of uniaxial magnets,

$$u = \frac{\mu_0 M_s}{2} [A(\nabla \mathbf{m})^2 + K(1 - m_z^2) + D\mathbf{m} \cdot ((\mathbf{p} \times \nabla) \times \mathbf{m})], \quad (2)$$

where A is the exchange constant, K is the easy-axis anisotropy along $\hat{\mathbf{z}}$, and D is the strength of the (interfacial-type) DMI with \mathbf{p} denoting the symmetry breaking direction. The dipolar interaction is not considered explicitly since, for the exchange type spin wave of interest in this work, its main role is to renormalize the anisotropy [32].

We suppose that the DMI is moderate with $D < D_c \equiv 4\sqrt{AK}/\pi$, hence the ground state is always the homogeneous magnetization $\mathbf{m} = \pm \hat{\mathbf{z}}$ with $u = 0$ [33]. Depending on the exact combinations of magnetic parameters A , K , and D , various magnetic textures such as domain walls [23], skyrmions [34], bobbars [35], and hopfions [36] may be stabilized with finite energy density $u > 0$.

When temporal evolution is involved, the total magnetization naturally divides into the slowly varying magnetic texture \mathbf{m}_0 and the fast oscillating spin wave \mathbf{m}' . Due to unity constraint $|\mathbf{m}| = 1$, the transverse condition $\mathbf{m}' \cdot \mathbf{m}_0 = 0$ is satisfied everywhere. Hence, we may define the spherical coordinates $\hat{\mathbf{e}}_{r,\theta,\phi}$ adhered to texture magnetization $\hat{\mathbf{e}}_r \equiv \mathbf{m}_0$, and describe the spin wave as $\mathbf{m}' = m_\theta \hat{\mathbf{e}}_\theta + m_\phi \hat{\mathbf{e}}_\phi$.

B. Spin wave density and flux

Before entering into explicit formulations regarding the actions on magnetic texture, we make the following observations for spin waves: (i) In uniaxial ferromagnets of interest here, spin waves can always be treated as right-circularly polarized, even when traveling upon inhomogeneous magnetic texture. The special form of magnon superfluidity involves spin waves in easy-plane magnets [37,38], thus it is beyond the scope of this work. (ii) Because of much faster oscillation of spin waves, preprocessing spin wave information in each oscillation period does not affect the remarkably slower dynamics of magnetic texture.

Based on the above observations, we proceed to extract time-invariant information from a fast oscillating spin wave. Note that first-order correlations vanish, $\langle m_{\theta/\phi} \rangle = 0$, where $\langle \cdots \rangle$ denotes the time-averaging evaluation. Meanwhile, second-order spin wave correlations yield

$$\langle m_\theta^2 \rangle = \langle m_\phi^2 \rangle = \rho, \quad (3a)$$

$$\langle m_\phi \nabla m_\theta \rangle = -\langle m_\theta \nabla m_\phi \rangle = \frac{\mathbf{j}}{2\gamma A}, \quad (3b)$$

where $\rho = \langle \mathbf{m}' \cdot \mathbf{m}' \rangle / 2$ and $\mathbf{j} = \gamma A \langle \nabla \mathbf{m}' \times \mathbf{m}' \rangle \cdot \mathbf{m}_0$ are the spin wave density and flux, respectively. Besides, other correlations include $\langle m_\theta m_\phi \rangle = 0$ and $\langle m_\theta \nabla m_\theta \rangle = \langle m_\phi \nabla m_\phi \rangle = \nabla \rho / 2$.

C. Magnonic torques

By partitioning into magnetic texture \mathbf{m}_0 and spin wave \mathbf{m}' , the total magnetization reads $\mathbf{m} = \sqrt{1 - \mathbf{m}' \cdot \mathbf{m}' } \mathbf{m}_0 + \mathbf{m}'$ in the small amplitude limit of the spin wave, $|\mathbf{m}'| \ll 1$, where the magnitude of the texture magnetization \mathbf{m}_0 is subject to a reduction factor $\sqrt{1 - \mathbf{m}' \cdot \mathbf{m}'}$ as enforced by unity constraint $|\mathbf{m}| = 1$. In accordance with above partition scheme, the LLG equation (1) is recast to

$$\dot{\mathbf{m}}_0 - \alpha \mathbf{m}_0 \times \dot{\mathbf{m}}_0 = \boldsymbol{\tau}_0 + \boldsymbol{\tau}, \quad (4)$$

where $\boldsymbol{\tau}_0 = \gamma \mathbf{h}(\mathbf{m}_0) \times \mathbf{m}_0$ is the torque caused by texture gyration and distortion, and $\boldsymbol{\tau}$ is the magnonic torque mediated by spin wave \mathbf{m}' . Performing time averaging and utilizing the spin wave correlations in Eq. (3), the magnonic torque $\boldsymbol{\tau}$ is then described by (see Appendix A for detailed mathematical derivations of all four torques below)

$$\begin{aligned} \boldsymbol{\tau} &= \boldsymbol{\tau}_{\text{STT}} + \boldsymbol{\tau}_{\text{DM}} + \boldsymbol{\tau}_{\text{GL}} + \boldsymbol{\tau}_{\text{PL}} \\ &= (\mathbf{j} \cdot \nabla) \mathbf{m}_0 - \frac{D}{2A} (\mathbf{p} \times \mathbf{j}) \times \mathbf{m}_0 \\ &\quad - 2\rho \gamma \mathbf{h}(\mathbf{m}_0) \times \mathbf{m}_0 - \gamma A (\nabla \rho \cdot \nabla) \mathbf{m}_0 \times \mathbf{m}_0, \end{aligned} \quad (5)$$

where the first and second terms are the spin-transfer torque (STT) and Dzyaloshinskii-Moriya (DM) torque mediated by the spin wave flux \mathbf{j} , and third and fourth terms are gravity-like (GL) and pressure-like (PL) torques mediated by the spin wave density ρ , respectively.

The spin-transfer torque $\boldsymbol{\tau}_{\text{STT}}$ is due to the tracking of spin wave precession to the inhomogeneous texture magnetization [28,29], similar to the process of electron spin tracking the background magnetization direction. The DM torque $\boldsymbol{\tau}_{\text{DM}}$ can be regarded as an extension of the spin transfer torque in the spirit of the chiral derivative [39,40]: $\partial_\beta \rightarrow \partial_\beta - (D/2A)(\mathbf{p} \times \hat{\mathbf{e}}_\beta) \times$, and is analogous to the Rashba torque in the electronic case [30]. The gravity-like torque $\boldsymbol{\tau}_{\text{GL}}$ is caused by the rescaling of the texture magnetization $(1 - \rho)\mathbf{m}_0$ in the presence of spin wave \mathbf{m}' [25]. The pressure-like torque $\boldsymbol{\tau}_{\text{PL}}$ is caused by the inhomogeneous spin wave distribution [31], and is intimately related to the entropic torque [15,41].

In a homogeneous domain with $\mathbf{m}_0 = \pm \hat{\mathbf{z}}$, only the DM torque in Eq. (5) survives, for a proper combination of the spin wave current \mathbf{j} , symmetry breaking direction \mathbf{p} , and magnetization \mathbf{m}_0 . The specific form of DM torque indicates that the spin wave flux \mathbf{j} generates an effective magnetic field

TABLE I. Hierarchy of magnonic driving models.

Level	Core approach	Reference	Complexity				
			Spin wave		Magnetic texture		Interaction
			Time	Space	Time	Space	
Wave	—	LLG equation (1)	✓	✓	—	✓	✓
Torque	Time averaging	Eq. (5), Refs. [28–31]	✗	✓	—	✓	✓
Force	Thiele equation	Eq. (7), Refs. [44,45]	✗	✓	—	✗	✓
Particle	Spin wave packet	Refs. [24–27]	✗	✗	—	✗	✓
Momentum	Noether theorem	Refs. [11,14,18,23]	—	—	—	✗	✗

$\mathbf{h}_D = -(D/2\gamma A)(\mathbf{p} \times \mathbf{j})$ acting on the static magnetization \mathbf{m}_0 , and further leads to a small magnetization tilting [30] (see also Appendix D). For bulk-type DMI instead of the interfacial type here, the DM torque is simply replaced by $\boldsymbol{\tau}_{\text{DM}} = (D/2A)\mathbf{j} \times \mathbf{m}_0$.

When the inhomogeneous distribution of spin wave density is purely induced by magnetic damping, the following relation is satisfied: $\nabla \rho \approx -(\alpha d/2)(\mathbf{j}/\gamma A)$, where d is the system dimension [31]. For this purely dissipative case, the pressure-like torque is alternatively written as [29,31]

$$\boldsymbol{\tau}_{\text{PL}} = \frac{\alpha d}{2}(\mathbf{j} \cdot \nabla)\mathbf{m}_0 \times \mathbf{m}_0 = \frac{\alpha d}{2}\boldsymbol{\tau}_{\text{STT}} \times \mathbf{m}_0, \quad (6)$$

which serves as a dissipative (or nonadiabatic) correction [42,43] to the (adiabatic) spin-transfer torque with a factor $\alpha d/2$. The nonadiabatic nature of $\boldsymbol{\tau}_{\text{PL}}$ in Eq. (6) originates from the slight mistracking of spin wave precession to the background magnetization variation, which we attribute to the response lag caused by magnetic damping.

D. Generalized Thiele equation

As seen in Eqs. (4) and (5), trimming the actions of rapidly oscillating spin waves into several magnonic torques markedly reduces the complexity of magnetic dynamics. Since magnetic texture tends to maintain its shape, further complexity reduction can be achieved by capturing the magnetic texture dynamics via the evolution of collective coordinates $\{X_\mu\}$ with $\mu = 1, 2, 3, \dots$, i.e., $\mathbf{m}_0(t) \equiv \mathbf{m}_0[\{X_\mu(t)\}]$. Specifically, left multiplying $\partial_\mu \mathbf{m}_0 \times \mathbf{m}_0$ to Eq. (4) and integrating in the whole magnetic volume \mathcal{V} yields the generalized Thiele equation [44,45],

$$B_{\mu\nu}^0 \dot{X}_\nu + E_\mu^0 - \alpha \Lambda_{\mu\nu}^0 \dot{X}_\nu = \int [(b_{\mu\beta}^0 + b_{\mu\beta}^D)j_\beta + 2e_\mu^0 \rho + \gamma A \lambda_{\mu\beta}^0 \partial_\beta \rho] d\mathcal{V}, \quad (7)$$

where μ and ν are indices reserved for collective coordinates of magnetic texture, β is for Cartesian coordinates, and the Einstein summation rule on repeated indices is implied. Here $b_{\mu\beta}^0 = \mathbf{m}_0 \cdot (\partial_\mu \mathbf{m}_0 \times \partial_\beta \mathbf{m}_0)$ and $b_{\mu\beta}^D = (D/2A)(\mathbf{p} \times \hat{\mathbf{e}}_\beta) \cdot \partial_\mu \mathbf{m}_0$ are the fictitious magnetic fields caused by the magnetic topology and DMI [25,46,47], $e_\mu^0 = -(\gamma/\mu_0 M_s) \partial_\mu u_0$ is the fictitious electric field caused by the inhomogeneous magnetic energy density [25,48], and $\lambda_{\mu\beta}^0 = \partial_\mu \mathbf{m}_0 \cdot \partial_\beta \mathbf{m}_0$ is the adhesion field characterizing the “roughness” of the nonuniform magnetizations. The global quantities denoted in upper case follow the definitions of the above local

quantities in lower case, i.e., $B_{\mu\nu}^0 = \int b_{\mu\nu}^0 d\mathcal{V}$, $E_\mu^0 = \int e_\mu^0 d\mathcal{V}$, and $\Lambda_{\mu\nu}^0 = \int \lambda_{\mu\nu}^0 d\mathcal{V}$. Alternatively for magnetic texture, $B_{\mu\nu}^0$ is the gyroscopic coefficient correlated with the topology charge, $E_\mu^0 = -(\gamma/\mu_0 M_s) \partial_\mu U_0$ is the restoration force, and $\alpha \Lambda_{\mu\nu}^0$ is the viscous coefficient.

In Eq. (7), all magnonic torques are transformed to forces mediated by the fictitious fields generated by the magnetic texture (see Appendix B for detailed discussions): the spin-transfer torque $\boldsymbol{\tau}_{\text{STT}}$ and the DM torque $\boldsymbol{\tau}_{\text{DM}}$ to Ampère forces, the gravity-like torque $\boldsymbol{\tau}_{\text{GL}}$ to electrostatic force, and the pressure-like torque $\boldsymbol{\tau}_{\text{PL}}$ to adhesion force. Note that the two sides of Eq. (7) share the same fields b^0 , e^0 , and λ^0 , reminding one that magnetic texture and spin waves are under the same magnetic environment. The only unpaired force is due to the additional field b^D , which highlights the unique role of DMI in shaping magnetic dynamics. Indeed, DMI is a key ingredient that introduces chirality to magnetic texture [49], and nonreciprocity to spin waves [50,51].

By decomposing a continuous spin wave into discrete spin wave packets, Ampère forces exerted by flux j in Eq. (7) are divided into Lorentz forces exerted by moving charges. Consequently, the interplay between spin wave packets and magnetic texture mimics the collision between two particle-like objects, as established in Ref. [25].

E. Hierarchy of magnonic driving models

From the preceding discussions, a hierarchy of magnonic driving models can be constructed by making more and more simplifications in each stage, as listed in Table I. Note that above five models lie at different levels of complexity, and thus have their own advantages and limitations in handling specific problems.

III. DOMAIN WALL MOTION INDUCED BY MAGNOMIC TORQUES

In the following, we scrutinize the torque model established in the preceding section by investigating the spin-wave-driven domain wall motion in a magnetic wire, where both DMI and magnetic damping are present. Specifically, the DMI breaks the rotational symmetry, and the magnetic damping breaks the translational symmetry in both space and time. While the momentum model hinging on symmetry preservation is no longer applicable, the microscopic torque model naturally fits into such investigations.

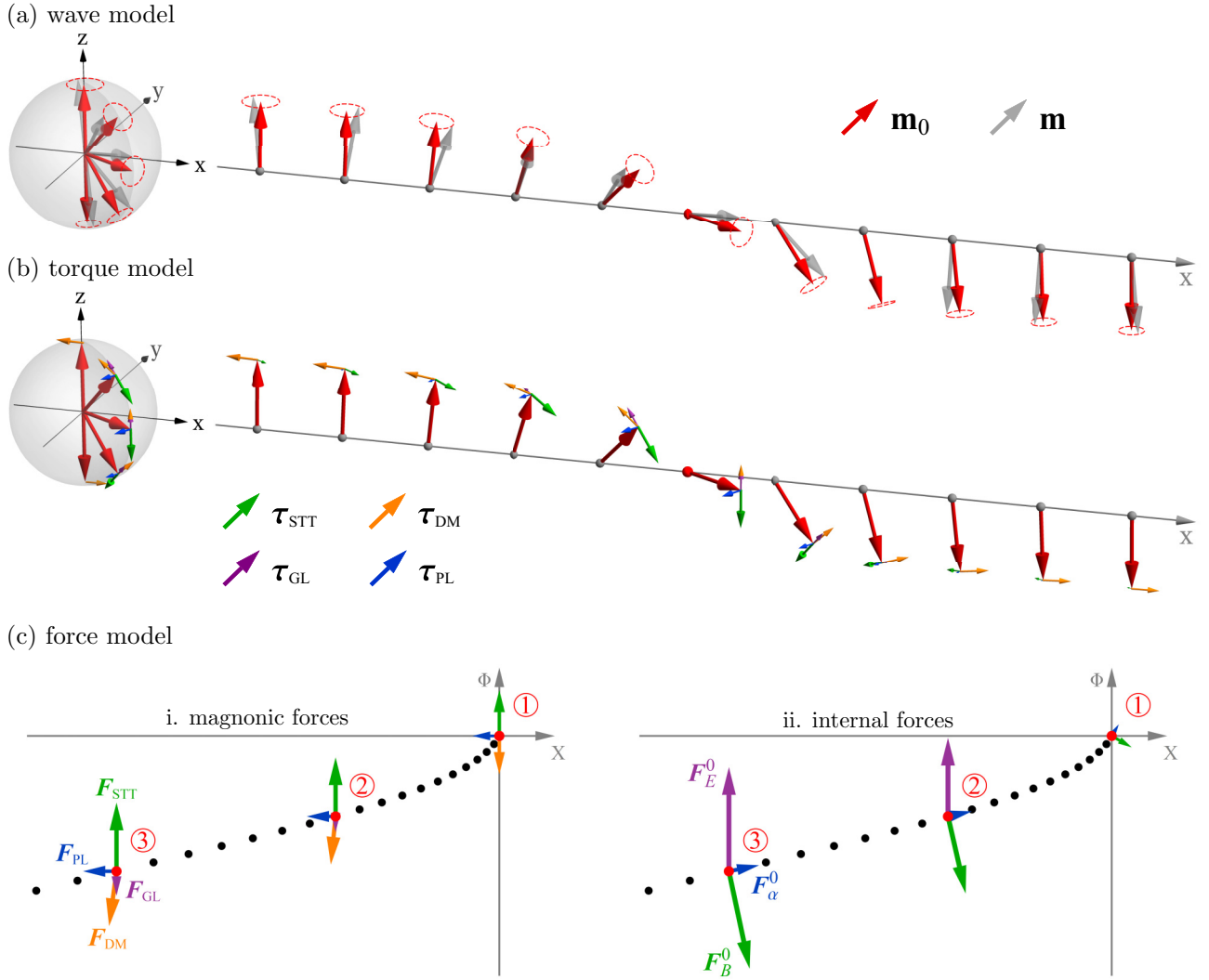


FIG. 1. Schematics of the domain wall dynamics induced by (a) spin waves, (b) the equivalent magnonic torques, and (c) magnonic forces. In (a) and (b), the red arrows depict the domain wall magnetizations, and all magnetizations are united in a magnetic Bloch sphere. For (a) the red circles represent the precessing spin waves, and for (b) the green/orange/purple/blue arrows represent the corresponding magnonic torques. In (c), the arrows depict the magnonic/internal forces (see Appendix B for definitions) in the left/right panels at three selected times. The black dots plot the time evolution of the domain wall in parametric space $\{X, \Phi\}$, and the red dots depict the three observation points.

A. Theoretical formulations

Consider a magnetic wire extending in the x axis, where the easy axis of the anisotropy and the symmetry-breaking direction of DMI both lie in the z axis. The ground states are magnetic domains with $\mathbf{m}_0 = \pm \hat{z}$, and the domain wall lying in between two domains is of Néel type as enforced by DMI, as seen in Fig. 1. More explicitly, the domain wall takes the Walker profile with $\theta_0 = 2 \arctan[\exp(x/W)]$ and $\phi_0 = 0$, where θ_0 and ϕ_0 are the polar and azimuthal angles of \mathbf{m}_0 about \hat{z} , and $W = \sqrt{A/K}$ is the characteristic width. The domain wall energy is $u_0 = \mu_0 M_s K \operatorname{sech}^2(x/W)$, which is contributed by the exchange coupling and the anisotropy half by half. The slow variation of the domain wall can be described by

$$\theta_0(t) = 2 \arctan \left[\exp \left(\frac{x - X(t)}{W} \right) \right], \quad \phi_0(t) = \Phi(t), \quad (8)$$

where the central position X and rotation angle Φ constitute the minimal set of collective coordinates of the domain wall.

Denoting the spin wave by complex field $\psi = m_\theta - im_\phi$, the spin wave dynamics is recast from the LLG equation (1) to a Schrödinger-like equation,

$$\frac{i - \alpha}{\gamma} \dot{\psi} = \left(-A \partial_x^2 + K - \frac{2}{\mu_0 M_s} u_0 + \frac{D}{2W} m_0^x \right) \psi, \quad (9)$$

where two effective potentials arise due to the inhomogeneous domain wall profile and DMI. Since the reflection by the Pöschl-Teller type potential well $-(2/\mu_0 M_s)u_0$ is always absent, and the scattering by the additional potential $(D/2W)m_0^x$ is negligible except for extremely low frequency, as shown in Fig. 4 of Appendix C, here we suppose perfect spin wave transmission for all cases. Consequently, the spin wave traveling upon the domain wall governed by Eq. (9) simply takes a

decaying plane wave form,

$$\psi = c \exp(ikx - \kappa x - i\omega t), \quad (10)$$

where c is the amplitude, k and κ are the real and imaginary parts of the wave vector, and ω is the angular frequency. The spin wave dispersion is $(1 + i\alpha)\omega = \gamma[A(k + i\kappa)^2 + K]$, and the group velocity is $v \equiv \partial_k \omega = 2\gamma Ak$.

From above spin wave information in Eq. (10), the spin wave density is $\rho = (c^2/2) \exp(-2\kappa x)$, the spin wave flux is $j = 2\gamma \rho Ak = \rho v$, and the density gradient is $\partial_x \rho = -2\rho\kappa$. Therefore, the magnonic torques in Eq. (5) are explicitly given by

$$\begin{aligned} \boldsymbol{\tau} &= \boldsymbol{\tau}_{\text{STT}} + \boldsymbol{\tau}_{\text{DM}} + \boldsymbol{\tau}_{\text{GL}} + \boldsymbol{\tau}_{\text{PL}} \\ &= \rho v \left(\partial_x \mathbf{m}_0 + \frac{D}{2A} \mathbf{m}_0 \times \hat{\mathbf{y}} \right) \\ &\quad + 2\rho(\mathbf{m}_0 \times \gamma \mathbf{h}_0 - \kappa \gamma A \mathbf{m}_0 \times \partial_x \mathbf{m}_0), \end{aligned} \quad (11)$$

where all torques are proportional to the spin wave density ρ , i.e., lying in second order to the spin wave.

With magnonic torques in Eq. (11), the domain wall dynamics with collective coordinates X and Φ is recast from Eq. (7) to

$$\frac{\dot{X}}{W} - \alpha \dot{\Phi} = -\frac{\rho_0 v}{W} (1 - \tilde{D} \cos \Phi) + (1 - 2\rho_0) \frac{v}{W} \frac{\tilde{D} \sin \Phi}{2kW}, \quad (12a)$$

$$\dot{\Phi} + \frac{\alpha \dot{X}}{W} = 2\kappa \rho_0 v \left(\tilde{D} \sin \Phi - \frac{\varepsilon}{2kW} \right), \quad (12b)$$

where $\rho_0 = \rho_s \exp[-2\kappa(X - x_s)]$ is the spin wave density at the domain wall center, and x_s and ρ_s are the position and spin wave density of the spin wave source, respectively.

In Eq. (12b), a correction factor $\varepsilon = 3/2$ is artificially introduced to take account of the domain wall dynamics beyond the parametric space $\{X, \Phi\}$. As seen in Appendix D, the DM torque tends to tilt the magnetization out of the domain wall plane, with the tilting magnitude proportional to local spin wave density. This tilting adds to the overall rotation of the domain wall, and thus leads to complicated distortion as formulated in Eq. (D4).

Noting that $\kappa \approx \alpha\omega/v$ for small damping $\alpha \ll 1$, the leading order of the domain wall motion in \dot{X} (rotation in $\dot{\Phi}$) then lies at the zeroth (first) order of the damping constant α . In this regard, the domain wall motion in \dot{X} is mainly contributed by spin transfer torque $\boldsymbol{\tau}_{\text{STT}}$, DM torque $\boldsymbol{\tau}_{\text{DM}}$, and internal torque $\boldsymbol{\tau}_0$, while the contribution of $\boldsymbol{\tau}_{\text{GL}}$ is negligible due to smallness of rotation angle $\Phi \ll 1$ and spin wave density $\rho \ll 1$. In the meantime, beside the contribution of DM torque $\boldsymbol{\tau}_{\text{DM}}$ and pressure-like torque $\boldsymbol{\tau}_{\text{PL}}$ induced by the spin wave attenuation, the hybridization term between X and Φ also manifests as a crucial ingredient in the rotating domain wall. Alternatively, Eq. (12) can be interpreted as a balance between external magnonic forces and internal texture forces, as elaborated in Appendix B.

The spin wave in Eq. (10) together with the corresponding magnonic torques formulated in Eq. (11) and the magnonic forces formulated in Eq. (B3) are schematically depicted in Fig. 1. Note that by converting spin wave to magnonic torques and further to magnonic forces, the driving scenarios become

increasingly transparent. For the torque model in Fig. 1(b), both the spin transfer torque $\boldsymbol{\tau}_{\text{STT}}$ and gravity-like torque $\boldsymbol{\tau}_{\text{GL}}$ tend to move the domain wall, while the pressure-like torque $\boldsymbol{\tau}_{\text{PL}}$ tends to rotate the domain wall. Meanwhile, the DM torque $\boldsymbol{\tau}_{\text{DM}}$ competes with all these torques in both domain wall motion and rotation. The above relations between magnonic torques are corroborated by the force model in Fig. 1(c), where the participation of DMI in both dynamics of X and Φ is unambiguously indicated by the tilting of \mathbf{F}_{DM} . In addition, the tilting of both \mathbf{F}_b^0 and \mathbf{F}_a^0 also highlight the dynamics hybridization between X and Φ , due to the gyroscopic nature of ferromagnetic dynamics.

B. Numerical results

To quantitatively investigate the domain wall dynamics, we carry out three types of numerical calculations in parallel: (i) wave-based analysis, by performing micromagnetic simulations using the original LLG equation (1) with the spin wave included; (ii) torque-based analysis, by performing micromagnetic simulations using the equivalent magnonic torques in Eq. (11); and (iii) force-based analysis, by seeking numerical solutions to the collective coordinate equation (12). For micromagnetic simulations in wave- and torque-based analyses, a micromagnetic module developed by Yu *et al.* [52] is employed, where the LLG equation is transformed to a weak form, and solved by the generalized-alpha method. The magnetic parameters are mainly based on yttrium iron garnet (YIG) [9,53]: the exchange coupling constant $A = 3.28 \times 10^{-11}$ A m, the easy-axis anisotropy $K = 3.88 \times 10^4$ A m⁻¹, the saturation magnetization $M_s = 1.94 \times 10^5$ A m⁻¹, the gyromagnetic ratio $\gamma = 2.21 \times 10^5$ m A⁻¹s⁻¹, and the vacuum permeability $\mu_0 = 1.26 \times 10^{-6}$ T m A⁻¹.

When damping is negligible, $\kappa = \alpha = 0$, domain wall is subject to no rotation ($\Phi = 0$) according to Eq. (12b), and the domain wall velocity is simply given by

$$V \equiv \dot{X} = -\eta \rho_s v, \quad (13)$$

where $\eta = 1 - \tilde{D}$. The scaling factor η originates from the rotational symmetry breaking induced by DMI, as we note that the relation $V = -\rho_s v$ at $D = 0$ is a manifestation of angular momentum conservation [14]. The slowdown of the domain wall motion by DMI is clearly shown in Fig. 2(a), for a series of DM strengths. Moreover, the factor η extracted at different spin wave frequencies also coincides well with the theoretical expectation in Eq. (13). Nevertheless, slight deviation from Eq. (13) is spotted as D approaches D_c (or η approach 0), which we attribute to the increasing instability toward a spin spiral state.

When magnetic damping is finite, $\alpha \neq 0$, but the DMI is absent, $D = 0$, the domain wall velocity is simply described by $V = -\rho_0 v$, according to Eq. (12a). However, due to spin wave attenuation, the domain wall experiences larger magnonic torque as its approaches the spin wave source. As a result, domain wall velocity is modulated by $\dot{V}/V = \dot{\rho}_0/\rho_0 = -2\kappa V$, i.e., the domain wall is subject to an effective drag force with coefficient 2κ . Consequently, the domain wall ve-

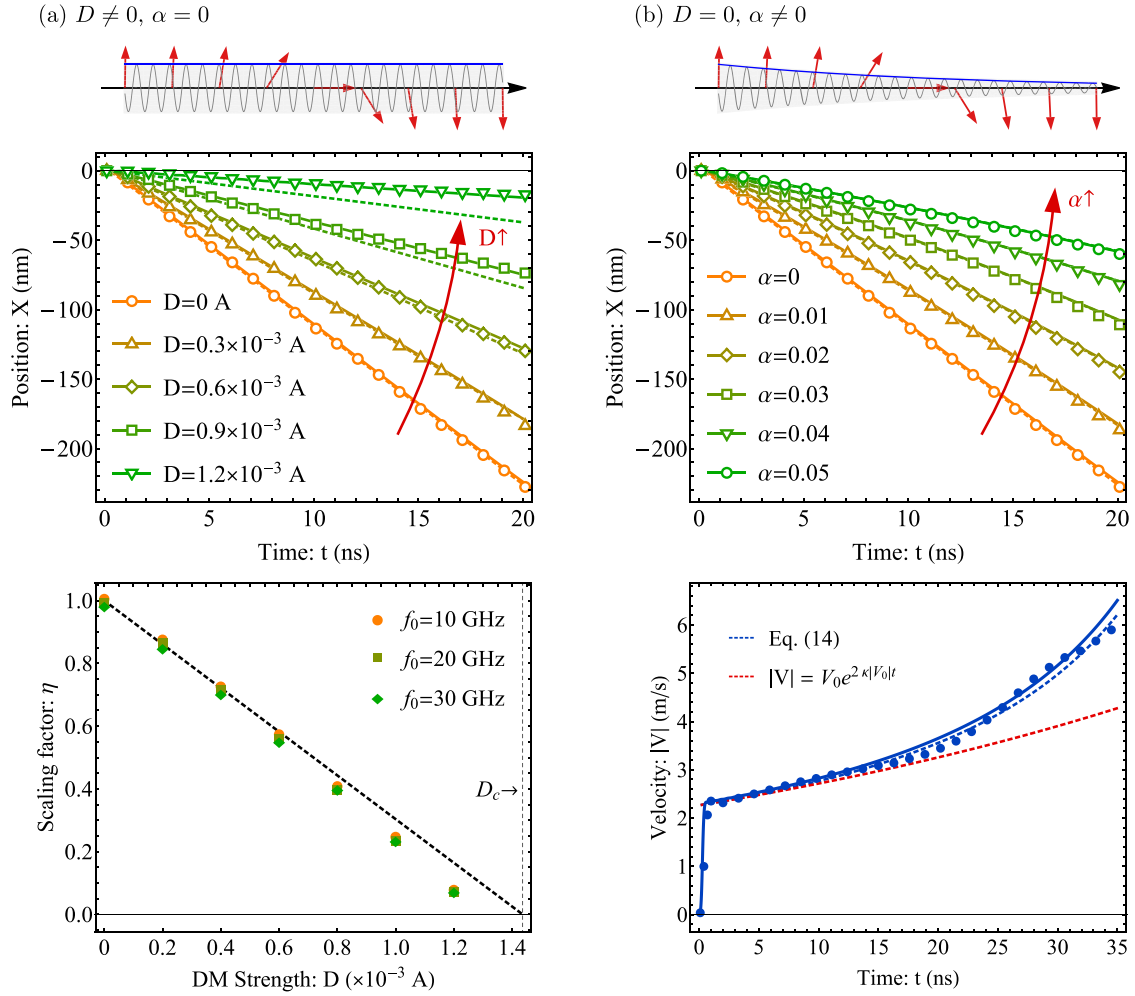


FIG. 2. Spin-wave-driven domain wall motion under (a) $D \neq 0, \alpha = 0$ and (b) $D = 0, \alpha \neq 0$. In (a), the upper panel plots the time evolution of domain wall position under a set of different DM strengths D , and the lower panel plots the scaling factor η as function of DM strength. In (b), the upper panel plots the time evolution of domain wall position under a set of magnetic dampings α , the lower panel plots the domain wall velocity V for a relatively long time. For all plots, the dots/solid lines are extracted from micromagnetic simulations based on the original LLG equation (1) and the magnonic torques (11), and the dashed lines are based on Eq. (12). The spin wave is excited at $x_0 = -300$ nm with excitation frequency $f = 10$ GHz and spin wave density $\rho_0 = 0.02$.

locity is explicitly described by [27]

$$V = -\frac{|V_0|}{1 - 2\kappa|V_0|t}, \quad (14)$$

where $V_0 = -\rho_s v \exp[-2\kappa(X_0 - x_s)]$ is the domain wall velocity at initial position X_0 . For a short time $t \ll t_0 \equiv 1/2\kappa|V_0| \approx 55$ ns, the domain wall velocity is almost invariant in time, and decreases exponentially as damping constant α increases, as depicted in Fig. 2(b). For a long time $t \sim t_0$, the domain wall velocity increases reciprocally as formulated in Eq. (14), deviating from an empirically anticipated exponential law $V = -|V_0| \exp(2\kappa|V_0|t)$.

Although both the DMI and the damping slow down the domain wall motion driven by the spin wave in Fig. 2, their roles are distinct from the viewpoint of symmetry. The main role of DMI is to generate a DM torque that counteracts the spin-transfer torque, i.e., the underlying mechanism is the rotational symmetry breaking. In contrast, the role of damping is to attenuate the spin wave and thus decrease the spin wave density (flux) touching the domain

wall, i.e., the underlying mechanism is translational symmetry breaking.

When sizable DMI and magnetic damping are both present with $D \neq 0$ and $\alpha \neq 0$, the evolution of domain wall velocity becomes more complicated, due to competitions and correlations between multiple torques in Eq. (11). Despite these complexities, the evolution of domain wall velocity is quantitatively reproduced by both torque-based simulations and force-based analyses, as shown in Fig. 3(a). Furthermore, according to Eq. (12), the overall domain wall velocity naturally splits into three different parts: V_{STT} by spin transfer torque, V_{DM} from DM torque, V_Φ from the internal restoration torque. A small contribution from gravity-like torque also appears in Eq. (12b), but can be neglected due to the smallness of both rotation angle Φ and spin wave density ρ . Among these contributions, V_{STT} and V_{DM} are much larger, and remain as the major part even after mutual cancellation, while V_Φ driven by finite angle Φ is also noteworthy, even though no spin wave reflection is included here. To further investigate the driving mechanism, the rotation angle Φ is also divided into two parts

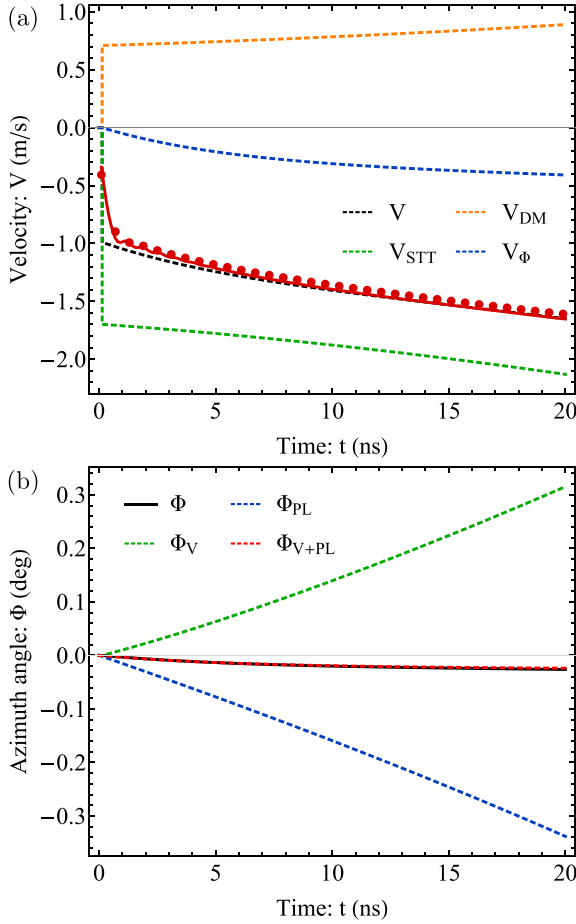


FIG. 3. Time evolution of (a) domain wall velocity V and (b) angle Φ under $D = 0.6 \times 10^{-3}$ A and $\alpha = 0.05$. The dots are for wave-based analysis using Eq. (1), the solid lines are for torque-based analysis using Eq. (11), and dashed lines are for force-based analysis using Eq. (12), respectively.

in Fig. 3(b): Φ_V caused by dynamics hybridization between X and Φ , and Φ_{PL} caused by pressure-like torque τ_{PL} . While Φ_V and Φ_{PL} always tend to cancel out with each other, the accumulation of the small mismatch gives rise to a small but gradually increasing rotation angle Φ , and further modifies the domain wall velocity via V_Φ in Fig. 3(a).

IV. DISCUSSIONS AND CONCLUSION

The magnonic torque in Eq. (5) shares many similarities with its electronic counterpart, as manifested in the spin transfer torque and the DM (Rashba) torque, because both spin wave and spin-polarized conduction electrons are angular momentum carriers [1]. However, different from the electric nature of conduction electron, the magnetic nature of spin waves adds several new flavors to magnonic torques: (i) Unlike conduction electrons, spin waves share the same magnetic degree of freedom with the background magnetization, and thus the gravity-like and pressure-like magnonic torques additionally emerge. (ii) The intrinsic magnetic nature of the spin wave implies its sensitivity to magnetic environment,

therefore the spatial distribution of spin waves and further magnonic torques can be quite complicated due to magnetic scattering. In contrast, the electric current can be regarded as uniform in the length scale of magnetic texture, giving rise to a much simpler form of its electronic counterpart. (iii) Due to relatively slow spin wave propagation, a finite time is required for magnonic torque to act on the whole magnetic texture, as demonstrated in Figs. 2 and 3; Given the extremely high propagation speed of electric current, such a response time is negligible.

In this work, the validity of magnonic torques rests with the circularly polarized form of the spin wave, which is ensured when exchange coupling is dominating. However, when hard-axis anisotropy is remarkable in biaxial ferromagnets, the spin wave is squeezed to elliptical form [54]. Furthermore, in antiferromagnets and ferrimagnets, the spin wave is endowed with full polarization degree of freedom [5,12,47,55,56] and may take arbitrary polarization including all circular, linear, and elliptical forms. To account for these complications, polarization and other relevant information beside the spin wave density and flux are necessary to fully describe the magnonic torques. The above information would also be added as ingredients to further distinguish the magnonic torque from its electronic counterpart.

In conclusion, by converting the action of spin waves to a set of magnonic torques, we established torque model to formulate the general dynamics of magnetic texture induced by spin waves. Via the torque-based simulations and force-based analyses, the domain wall motion driven by spin waves is systematically investigated, even though the translational and rotational symmetries are broken by DMI and magnetic damping, respectively. With unique features and transparent meanings of these magnonic torques, more delicate manipulations of magnetic texture using spin waves are envisioned.

ACKNOWLEDGMENTS

J.L. is grateful to Jiang Xiao for insightful discussions. This work is supported by the National Natural Science Foundation of China (Grant No. 11904260) and the Natural Science Foundation of Tianjin (Grant No. 20JCQNJC02020).

APPENDIX A: DERIVATION OF MAGNONIC TORQUES

When spin wave \mathbf{m}' travels upon magnetic texture \mathbf{m}_0 , the total magnetization subject to unity constraint $|\mathbf{m}| = 1$ is described by

$$\begin{aligned} \mathbf{m} &= \sqrt{1 - \mathbf{m}' \cdot \mathbf{m}'} \mathbf{m}_0 + \mathbf{m}' \\ &\approx \left(1 - \frac{\mathbf{m}' \cdot \mathbf{m}'}{2}\right) \mathbf{m}_0 + \mathbf{m}' \\ &= \mathbf{m}_0 + \mathbf{m}' - \rho \mathbf{m}_0, \end{aligned} \quad (\text{A1})$$

which corresponds to zeroth-, first-, and second-order terms in spin wave \mathbf{m}' . Meanwhile, the effective magnetic field is

$$\mathbf{h}(\mathbf{m}) = A \nabla^2 \mathbf{m} + K_m \hat{z} - D(\mathbf{p} \times \nabla) \times \mathbf{m}, \quad (\text{A2})$$

which naturally splits into three parts, $\mathbf{h}(\mathbf{m}) = \mathbf{h}(\mathbf{m}_0) + \mathbf{h}(\mathbf{m}') - \mathbf{h}(\rho \mathbf{m}_0)$, according to Eq. (A1). Furthermore, the

effective field has the following property:

$$\mathbf{h}(\rho\mathbf{m}_0) - \rho\mathbf{h}(\mathbf{m}_0) \approx 2A(\nabla\rho \cdot \nabla)\mathbf{m}_0 - D(\mathbf{p} \times \nabla)\rho \times \mathbf{m}_0, \quad (\text{A3})$$

which is caused by the fact that $\partial_\beta(\rho\mathbf{m}_0) - \rho\partial_\beta\mathbf{m}_0 = (\partial_\beta\rho)\mathbf{m}_0$.

Inserting Eq. (A1) to the LLG equation (1) yields

$$\begin{aligned} \dot{\mathbf{m}}_0 - \alpha\mathbf{m}_0 \times \dot{\mathbf{m}}_0 = & -\mathbf{m}_0 \times \gamma\mathbf{h}(\mathbf{m}_0) - \mathbf{m}' \times \gamma\mathbf{h}(\mathbf{m}') \\ & + \rho\mathbf{m}_0 \times \gamma\mathbf{h}(\mathbf{m}_0) + \mathbf{m}_0 \times \gamma\mathbf{h}(\rho\mathbf{m}_0), \end{aligned} \quad (\text{A4})$$

where only zeroth- and second-order terms in spin wave \mathbf{m}' are kept, and the first-order terms are dropped since they always average out in time evolution. On the right side of Eq. (A4), the first term is τ_0 caused by the texture distortion and gyration, and the remaining three items together constitute the magnonic torques τ . Inserting Eqs. (A2) and (A3) into Eq. (A4), the magnonic torque is then described by

$$\begin{aligned} \tau \approx & 2\rho\mathbf{m}_0 \times \gamma\mathbf{h}(\mathbf{m}_0) + \mathbf{m}_0 \times \gamma[2A(\nabla\rho \cdot \nabla)\mathbf{m}_0 \\ & - D(\mathbf{p} \times \nabla)\rho \times \mathbf{m}_0] - \langle \mathbf{m}' \times \gamma A \nabla^2 \mathbf{m}' \rangle \\ & + \langle \mathbf{m}' \times \gamma [D(\mathbf{p} \times \nabla) \times \mathbf{m}'] \rangle, \end{aligned} \quad (\text{A5})$$

where the time averaging $\langle \dots \rangle$ is used to further remove redundant fluctuations.

In the second line of Eq. (A5), the torque related to the exchange coupling is transformed to

$$\begin{aligned} -\langle \mathbf{m}' \times \gamma A \nabla^2 \mathbf{m}' \rangle = & -\partial_\beta \langle \mathbf{m}' \times \gamma A \partial_\beta \mathbf{m}' \rangle \\ = & \partial_\beta (j_\beta \mathbf{m}_0 + \gamma A \rho \partial_\beta \mathbf{m}_0 \times \mathbf{m}_0) \\ \approx & (\mathbf{j} \cdot \nabla) \mathbf{m}_0 + \gamma A (\nabla\rho \cdot \nabla) \mathbf{m}_0 \times \mathbf{m}_0, \end{aligned} \quad (\text{A6})$$

where following relation is employed:

$$\begin{aligned} \langle \mathbf{m}' \times \partial_\beta \mathbf{m}' \rangle &= (\mathbf{m}_0 \cdot \langle \mathbf{m}' \times \partial_\beta \mathbf{m}' \rangle) \mathbf{m}_0 + \mathbf{m}_0 \times (\langle \mathbf{m}' \times \partial_\beta \mathbf{m}' \rangle \times \mathbf{m}_0) \\ &= -\frac{j_\beta}{\gamma A} \mathbf{m}_0 + \langle (\mathbf{m}_0 \cdot \partial_\beta \mathbf{m}') (\mathbf{m}' \times \mathbf{m}_0) \rangle \\ &= -\frac{j_\beta}{\gamma A} \mathbf{m}_0 - \langle (\partial_\beta \mathbf{m}_0 \cdot \mathbf{m}') (\mathbf{m}' \times \mathbf{m}_0) \rangle \\ &= -\frac{j_\beta}{\gamma A} \mathbf{m}_0 - \rho \partial_\beta \mathbf{m}_0 \times \mathbf{m}_0. \end{aligned} \quad (\text{A7})$$

Similarly, the torque related to the DMI in third line of Eq. (A5) is transformed to

$$\begin{aligned} \langle \mathbf{m}' \times [\gamma D(\mathbf{p} \times \nabla) \times \mathbf{m}'] \rangle &= \langle \mathbf{m}' \times [\gamma D(\mathbf{p} \times \hat{\mathbf{e}}_\beta) \times \partial_\beta \mathbf{m}'] \rangle \\ &= -\langle [\gamma D(\mathbf{p} \times \hat{\mathbf{e}}_\beta) \cdot \mathbf{m}'] \partial_\beta \mathbf{m}' \rangle + \gamma D(\mathbf{p} \times \hat{\mathbf{e}}_\beta) \langle \mathbf{m}' \cdot \partial_\beta \mathbf{m}' \rangle \\ &\approx -\gamma D(\mathbf{p} \times \hat{\mathbf{e}}_\beta) \times \frac{j_\beta}{2\gamma A} \mathbf{m}_0 + \gamma D(\mathbf{p} \times \hat{\mathbf{e}}_\beta) \partial_\beta \rho \\ &= -\frac{D}{2A} (\mathbf{p} \times \mathbf{j}) \times \mathbf{m}_0 + \gamma D \mathbf{m}_0 \times [(\mathbf{p} \times \nabla)\rho \times \mathbf{m}_0]. \end{aligned} \quad (\text{A8})$$

In the derivation of Eqs. (A7) and (A8), we utilize the following properties for circularly polarized spin wave \mathbf{m}' , supposing that $\mathbf{c} = c_\theta \hat{\mathbf{e}}_\theta + c_\phi \hat{\mathbf{e}}_\phi$ is an arbitrary vector transverse to $\hat{\mathbf{e}}_r \equiv \mathbf{m}_0$:

$$\begin{aligned} \langle (\mathbf{c} \cdot \mathbf{m}') \mathbf{m}' \rangle &= \langle (c_\theta m_\theta + c_\phi m_\phi) (m_\theta \hat{\mathbf{e}}_\theta + m_\phi \hat{\mathbf{e}}_\phi) \rangle \\ &= \langle m_\theta^2 \rangle c_\theta \hat{\mathbf{e}}_\theta + \langle m_\phi^2 \rangle c_\phi \hat{\mathbf{e}}_\phi \\ &= \rho \mathbf{c}, \end{aligned} \quad (\text{A9a})$$

and similarly

$$\begin{aligned} \langle (\mathbf{c} \cdot \mathbf{m}') \partial_\beta \mathbf{m}' \rangle &\approx \langle (c_\theta m_\theta + c_\phi m_\phi) (\partial_\beta m_\theta \hat{\mathbf{e}}_\theta + \partial_\beta m_\phi \hat{\mathbf{e}}_\phi) \rangle \\ &\approx \langle m_\theta \partial_\beta m_\phi \rangle c_\theta \hat{\mathbf{e}}_\theta + \langle m_\phi \partial_\beta m_\theta \rangle c_\phi \hat{\mathbf{e}}_\theta \\ &= \frac{j_\beta}{2\gamma A} (\mathbf{c} \times \mathbf{m}_0). \end{aligned} \quad (\text{A9b})$$

Inserting Eqs. (A6) and (A8) into Eq. (A5), we then obtain the full set of magnonic torques in Eq. (5) of the main text. In the above derivations, we use $\mathbf{m}_0 \times (\dots \times \mathbf{m}_0)$ to extract the transverse components of magnonic torques with respect to texture magnetization \mathbf{m}_0 , to ensure the constant length of magnetization. In addition, several simplifications and approximations are utilized in the above derivations, to organize the magnonic torques in a compact and meaningful form.

APPENDIX B: MAGNONIC FORCES

The Thiele equation formulated in Eq. (7) can be rewritten in a force balance form, $F_\mu^0 + F_\mu = 0$. Here, F_μ^0 is the internal force experienced by magnetic texture in the parametric space $\{X_\mu\}$,

$$\begin{aligned} F_\mu^0 &= F_B^0 + F_E^0 + F_\alpha^0 \\ &= B_{\mu\nu}^0 \dot{X}_\nu + E_\mu^0 - \alpha \Lambda_{\mu\nu}^0 \dot{X}_\nu, \end{aligned} \quad (\text{B1})$$

and F_μ is the external magnonic force transformed from magnonic torques Eq. (5),

$$\begin{aligned} F_\mu &= F_{\text{STT}} + F_{\text{DM}} + F_{\text{GL}} + F_{\text{PL}} \\ &= - \int [(b_{\mu\beta}^0 + b_{\mu\beta}^D) j_\beta + 2e_\mu^0 \rho + \gamma A \lambda_{\mu\beta}^0 \partial_\beta \rho] dV. \end{aligned} \quad (\text{B2})$$

The Ampère force F_{STT} (electrostatic force F_{GL}) in Eq. (B2) and its dual partner F_B^0 (F_E^0) in Eq. (B1) share the same field b^0 (e^0), and they together serve to transfer angular and linear momenta between spin wave and magnetic texture. Meanwhile, the adhesion force F_{PL} and viscous force F_α^0 share the same adhesion field λ^0 , and they mimic the sliding friction between two contacting surfaces. After above pairing of external and internal forces, the Ampère force F_{DM} imposed on field b^D is left out as the only unpaired magnonic force, highlighting the unique role of DMI. When F_{DM} has nonzero overlap with F_{STT} or F_{GL} , it acts as an additional source for angular and linear momenta, i.e., momentum conservation is destroyed by DMI.

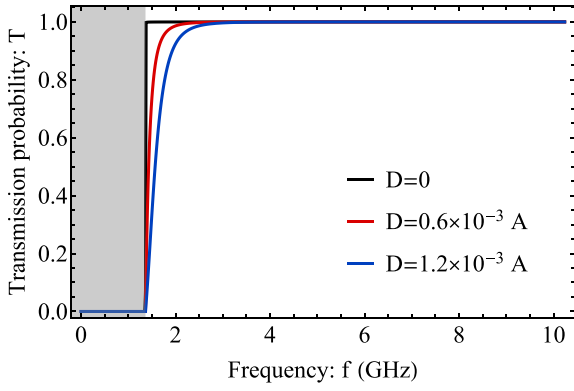


FIG. 4. Transmission probability of the spin wave across the domain wall under different DM strengths. The black/red/blue lines represent different DM strengths, and the gray shaded area denotes the frequency range below the gap.

Specifically for a domain wall, by inserting Eq. (8) into Eq. (B2) in parametric space $\{X, \Phi\}$, the magnonic forces $\mathbf{F} \equiv (F_X, F_\Phi)$ are explicitly given by

$$\mathbf{F}_{\text{STT}} = 2\rho_0 v(0, 1), \quad \mathbf{F}_{\text{DM}} = -2\rho_0 v(-2\kappa\tilde{D} \sin \Phi, \tilde{D} \cos \Phi), \quad (\text{B3a})$$

$$\mathbf{F}_{\text{GL}} = \rho_0(0, \pi\gamma D \sin \Phi), \quad \mathbf{F}_{\text{PL}} = -4\rho_0 \left(\frac{\kappa\gamma A}{W}, 0 \right), \quad (\text{B3b})$$

where ρ_0 denotes the spin wave density at the domain wall center, and $\tilde{D} = D/D_c$ is the normalized DM strength with $D_c = 4\sqrt{AK}/\pi$ the critical DM strength. In responses to above magnonic forces, the internal forces are

$$\mathbf{F}_B^0 = 2(-\dot{\Phi}, \dot{X}), \quad (\text{B4a})$$

$$\mathbf{F}_E^0 = (0, -\pi\gamma D \sin \Phi/2), \quad (\text{B4b})$$

$$\mathbf{F}_\alpha^0 = -2\alpha(\dot{X}/W, W\dot{\Phi}), \quad (\text{B4c})$$

where the gyroscopic coefficients are $B_{\Phi X}^0 = -B_{X\Phi}^0 = 2$, and the viscous coefficients are $\Lambda_{XX}^0 = 2/W$ and $\Lambda_{\Phi\Phi}^0 = 2W$. Collecting all forces above, the domain wall dynamics in Eq. (12) is reproduced.

APPENDIX C: SPIN WAVE TRANSMISSION ACROSS THE DOMAIN WALL

According to Eq. (9), the problem of spin wave scattering by the domain wall is equivalent to the problem of the electronic scattering by two effective potentials, hence it can be directly calculated via the Green function method [57]. The spin wave transmission across the domain wall is plotted in Fig. 4 under different strengths of DMI. When DMI is absent ($D = 0$), the transmission is always perfect; and even when DMI is sizable, only little reflection occurs for extremely low frequencies near the frequency gap.

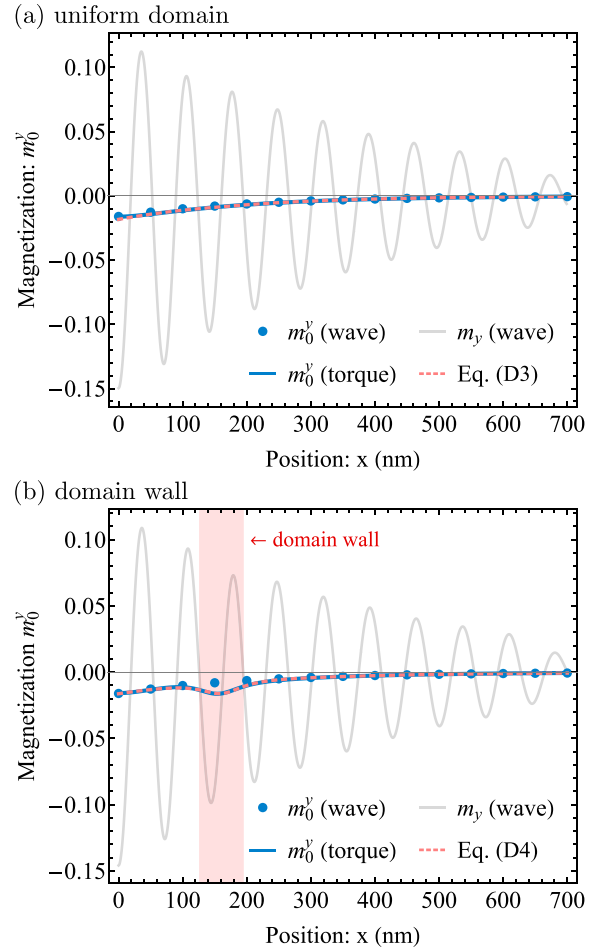


FIG. 5. Modification of magnetic profile by magnonic DM torque in (a) a uniform domain and (b) a domain wall. The gray solid line is for total magnetization m^y extracted from wave-based simulations, and all other lines (dots) are for the static magnetization m_0^y . The blue dots are from wave-based simulations, the blue solid line is from torque-based simulations, and the red dashed line is from theoretical equations (D3) and (D4). In all simulations and calculations, the DM strength is $D = 0.9 \times 10^{-3}$ A and the magnetic damping is $\alpha = 0.05$. The spin wave density is $\rho_0 = 9 \times 10^{-3}$ at the excitation point $x = 0$ nm, and all magnetic data are taken after a relaxation time of $t = 3$ ns.

APPENDIX D: ASYMMETRIC DOMAIN WALL PROFILE INDUCED BY DZIALOSHINSKII-MORIYA TORQUE

We first consider the case where the spin wave is traveling upon a uniform domain, in a magnetic wire along the x axis. The overall magnetic field experienced by the uniform magnetization is

$$\mathbf{h} = Km_0^z \hat{\mathbf{z}} - \frac{D}{2\gamma A} \rho v \hat{\mathbf{y}}, \quad (\text{D1})$$

where the former is the anisotropic field and the latter is effective field caused by magnonic DM torque according to Eq. (11).

At equilibrium, the magnetization aligns parallel to the magnetic field, $\mathbf{m}_0 \parallel \mathbf{h}$, or $m_0^y/m_0^z = h_y/h_z$, therefore the

magnetization is slightly tilted out in the \hat{y} direction with [30]

$$m_0^y \approx -\frac{D}{2\gamma AK} \rho v, \quad (\text{D2})$$

where only terms linear in ρ are retained. It is noteworthy that, to achieve the equilibrium magnetization state, finite magnetic damping ($\alpha \neq 0$) is required to release redundant energies. Therefore, the spin wave density ρ decays exponentially along x direction, and Eq. (D2) is further given by

$$m_0^y \approx -\frac{D}{2\gamma AK} \rho_s v \exp[-2\kappa(x - x_s)], \quad (\text{D3})$$

where ρ_s is the spin wave density at the excitation point x_s . Such a magnetization tilting is verified by both wave-based and torque-based simulations in Fig. 5(a).

We then move to the case where the spin wave is traveling upon a domain wall. Since the DM torque maintains the same form outside and inside the domain wall, we expect that the magnetization tilting in Eq. (D3) valid for both domains at

two sides naturally extends to the domain wall region. Hence, the full domain wall profile reads

$$m_0^y \approx \text{sech}\left(\frac{x - X}{W}\right) \sin \Phi - \frac{D}{2\gamma AK} \rho_s v \exp[-2\kappa(x - x_s)], \quad (\text{D4})$$

where the first term is the Walker profile defined at central position X and rotation angle Φ of the domain wall. As a result of DM torque, the domain wall profile apparently becomes asymmetric with respect to the central position X . In Fig. 5(b), the extra magnetization tilting is confirmed by the torque-based simulation. However, the magnetization tilting is not discernible in wave-based simulation, possibly due to relatively large and complicated spin wave oscillations. Nevertheless, the magnetization tilting in Eq. (D4) indicates that the domain wall dynamics induced by DM torque cannot be fully captured by Eq. (8) with only two collective coordinates X and Φ .

-
- [1] Y. Kajiwara, K. Harii, S. Takahashi, J. Ohe, K. Uchida, M. Mizuguchi, H. Umezawa, H. Kawai, K. Ando, K. Takanashi, S. Maekawa, and E. Saitoh, Transmission of electrical signals by spin-wave interconversion in a magnetic insulator, *Nature (London)* **464**, 262 (2010).
 - [2] L. J. Cornelissen, J. Liu, R. A. Duine, J. B. Youssef, and B. J. van Wees, Long-distance transport of magnon spin information in a magnetic insulator at room temperature, *Nat. Phys.* **11**, 1022 (2015).
 - [3] R. Lebrun, A. Ross, S. A. Bender, A. Qaiumzadeh, L. Baldrati, J. Cramer, A. Brataas, R. A. Duine, and M. Kläui, Tunable long-distance spin transport in a crystalline antiferromagnetic iron oxide, *Nature (London)* **561**, 222 (2018).
 - [4] J. Han, P. Zhang, J. T. Hou, S. A. Siddiqui, and L. Liu, Mutual control of coherent spin waves and magnetic domain walls in a magnonic device, *Science* **366**, 1121 (2019).
 - [5] Y. Nambu, J. Barker, Y. Okino, T. Kikkawa, Y. Shiomi, M. Enderle, T. Weber, B. Winn, M. Graves-Brook, J. M. Tranquada, T. Ziman, M. Fujita, G. E. W. Bauer, E. Saitoh, and K. Kakurai, Observation of Magnon Polarization, *Phys. Rev. Lett.* **125**, 027201 (2020).
 - [6] H. Wang, S. Zhang, N. J. McLaughlin, B. Flebus, M. Huang, Y. Xiao, C. Liu, M. Wu, E. E. Fullerton, Y. Tserkovnyak, and C. R. Du, Noninvasive measurements of spin transport properties of an antiferromagnetic insulator, *Sci. Adv.* **8**, eabg8562 (2022).
 - [7] A. V. Chumak, V. I. Vasyuchka, A. A. Serga, and B. Hillebrands, Magnon spintronics, *Nat. Phys.* **11**, 453 (2015).
 - [8] A. Barman, G. Gubbiotti, S. Ladak, A. O. Adeyeye, M. Krawczyk, J. Gräfe, C. Adelman, S. Cotozana, A. Naeemi, V. I. Vasyuchka, B. Hillebrands, S. A. Nikitov, H. Yu, D. Grundler, A. V. Sadovnikov, A. A. Grachev, S. E. Sheshukova, J.-Y. Duquesne, M. Marangolo, G. Csaba *et al.*, The 2021 magnonics roadmap, *J. Phys.: Condens. Matter* **33**, 413001 (2021).
 - [9] J. Lan, W. Yu, R. Wu, and J. Xiao, Spin-Wave Diode, *Phys. Rev. X* **5**, 041049 (2015).
 - [10] W. Yu, J. Lan, and J. Xiao, Magnetic Logic Gate Based on Polarized Spin Waves, *Phys. Rev. Appl.* **13**, 024055 (2020).
 - [11] W. Wang, M. Albert, M. Beg, M.-A. Bisotti, D. Chernyshenko, D. Cortés-Ortuño, I. Hawke, and H. Fangohr, Magnon-Driven Domain-Wall Motion with the Dzyaloshinskii-Moriya Interaction, *Phys. Rev. Lett.* **114**, 087203 (2015).
 - [12] W. Yu, J. Lan, and J. Xiao, Polarization-selective spin wave driven domain-wall motion in antiferromagnets, *Phys. Rev. B* **98**, 144422 (2018).
 - [13] D. R. Rodrigues, A. Salimath, K. Everschor-Sitte, and K. M. D. Hals, Spin-Wave Driven Bidirectional Domain Wall Motion in Kagome Antiferromagnets, *Phys. Rev. Lett.* **127**, 157203 (2021).
 - [14] P. Yan, X. S. Wang, and X. R. Wang, All-Magnonic Spin-Transfer Torque and Domain Wall Propagation, *Phys. Rev. Lett.* **107**, 177207 (2011).
 - [15] D. Hinzke and U. Nowak, Domain Wall Motion by the Magnonic Spin Seebeck Effect, *Phys. Rev. Lett.* **107**, 027205 (2011).
 - [16] M. Mochizuki, X. Z. Yu, S. Seki, N. Kanazawa, W. Koshibae, J. Zang, M. Mostovoy, Y. Tokura, and N. Nagaosa, Thermally driven ratchet motion of a skyrmion microcrystal and topological magnon Hall effect, *Nat. Mater.* **13**, 241 (2014).
 - [17] C. Jia, D. Ma, A. F. Schäffer, and J. Berakdar, Twisted magnon beams carrying orbital angular momentum, *Nat. Commun.* **10**, 2077 (2019).
 - [18] Y. Jiang, H. Y. Yuan, Z.-X. Li, Z. Wang, H. W. Zhang, Y. Cao, and P. Yan, Twisted Magnon as a Magnetic Tweezer, *Phys. Rev. Lett.* **124**, 217204 (2020).
 - [19] S. Lee and S. K. Kim, Orbital angular momentum and current-induced motion of a topologically textured domain wall in a ferromagnetic nanotube, *Phys. Rev. B* **104**, L140401 (2021).
 - [20] E. G. Tveten, A. Qaiumzadeh, and A. Brataas, Antiferromagnetic Domain Wall Motion Induced by Spin Waves, *Phys. Rev. Lett.* **112**, 147204 (2014).
 - [21] S. K. Kim, Y. Tserkovnyak, and O. Tchernyshyov, Propulsion of a domain wall in an antiferromagnet by magnons, *Phys. Rev. B* **90**, 104406 (2014).

- [22] S.-H. Oh, S. K. Kim, J. Xiao, and K.-J. Lee, Bidirectional spin-wave-driven domain wall motion in ferrimagnets, *Phys. Rev. B* **100**, 174403 (2019).
- [23] H. Yu, J. Xiao, and H. Schultheiss, Magnetic texture based magnonics, *Phys. Rep.* **905**, 1 (2021).
- [24] M. W. Daniels, W. Yu, R. Cheng, J. Xiao, and D. Xiao, Topological spin Hall effects and tunable skyrmion Hall effects in uniaxial antiferromagnetic insulators, *Phys. Rev. B* **99**, 224433 (2019).
- [25] J. Lan and J. Xiao, Skew scattering and side jump of spin wave across magnetic texture, *Phys. Rev. B* **103**, 054428 (2021).
- [26] Z. Jin, C. Y. Meng, T. T. Liu, D. Y. Chen, Z. Fan, M. Zeng, X. B. Lu, X. S. Gao, M. H. Qin, and J.-M. Liu, Magnon-driven skyrmion dynamics in antiferromagnets: Effect of magnon polarization, *Phys. Rev. B* **104**, 054419 (2021).
- [27] J. Lan and J. Xiao, Spin wave driven domain wall motion in easy-plane ferromagnets: A particle perspective, *Phys. Rev. B* **106**, L020404 (2022).
- [28] A. A. Kovalev and Y. Tserkovnyak, Thermomagnonic spin transfer and Peltier effects in insulating magnets, *Europhys. Lett.* **97**, 67002 (2012).
- [29] A. A. Kovalev, Skyrmionic spin Seebeck effect via dissipative thermomagnonic torques, *Phys. Rev. B* **89**, 241101(R) (2014).
- [30] A. Manchon, P. B. Ndiaye, J.-H. Moon, H.-W. Lee, and K.-J. Lee, Magnon-mediated Dzyaloshinskii-Moriya torque in homogeneous ferromagnets, *Phys. Rev. B* **90**, 224403 (2014).
- [31] S. K. Kim and Y. Tserkovnyak, Landau-Lifshitz theory of thermomagnonic torque, *Phys. Rev. B* **92**, 020410(R) (2015).
- [32] A. G. Gurevich and G. A. Melkov, *Magnetization Oscillations and Waves* (CRC, New York, 1990).
- [33] S. Rohart and A. Thiaville, Skyrmion confinement in ultrathin film nanostructures in the presence of Dzyaloshinskii-Moriya interaction, *Phys. Rev. B* **88**, 184422 (2013).
- [34] C. Back, V. Cros, H. Ebert, K. Everschor-Sitte, A. Fert, M. Garst, T. Ma, S. Mankovsky, T. L. Monchesky, M. Mostovoy, N. Nagaosa, S. S. P. Parkin, C. Pfleiderer, N. Reyren, A. Rosch, Y. Taguchi, Y. Tokura, K. von Bergmann, and J. Zang, The 2020 skyrmionics roadmap, *J. Phys. D: Appl. Phys.* **53**, 363001 (2020).
- [35] F. N. Rybakov, A. B. Borisov, S. Blügel, and N. S. Kiselev, New Type of Stable Particlelike States in Chiral Magnets, *Phys. Rev. Lett.* **115**, 117201 (2015).
- [36] B. Göbel, I. Mertig, and O. A. Tretiakov, Beyond skyrmions: Review and perspectives of alternative magnetic quasiparticles, *Phys. Rep.* **895**, 1 (2021).
- [37] S. K. Kim, S. Takei, and Y. Tserkovnyak, Topological spin transport by Brownian diffusion of domain walls, *Phys. Rev. B* **92**, 220409(R) (2015).
- [38] E. Iacocca, Controllable vortex shedding from dissipative exchange flows in ferromagnetic channels, *Phys. Rev. B* **102**, 224403 (2020).
- [39] K.-W. Kim, H.-W. Lee, K.-J. Lee, and M. D. Stiles, Chirality from Interfacial Spin-Orbit Coupling Effects in Magnetic Bilayers, *Phys. Rev. Lett.* **111**, 216601 (2013).
- [40] T. Kikuchi, T. Koretsune, R. Arita, and G. Tatara, Dzyaloshinskii-Moriya Interaction as a Consequence of a Doppler Shift due to Spin-Orbit-Induced Intrinsic Spin Current, *Phys. Rev. Lett.* **116**, 247201 (2016).
- [41] F. Schlickeiser, U. Ritzmann, D. Hinzke, and U. Nowak, Role of Entropy in Domain Wall Motion in Thermal Gradients, *Phys. Rev. Lett.* **113**, 097201 (2014).
- [42] S. Zhang and Z. Li, Roles of Nonequilibrium Conduction Electrons on the Magnetization Dynamics of Ferromagnets, *Phys. Rev. Lett.* **93**, 127204 (2004).
- [43] A. Thiaville, Y. Nakatani, J. Miltat, and Y. Suzuki, Micromagnetic understanding of current-driven domain wall motion in patterned nanowires, *Europhys. Lett.* **69**, 990 (2005).
- [44] A. A. Thiele, Steady-State Motion of Magnetic Domains, *Phys. Rev. Lett.* **30**, 230 (1973).
- [45] O. A. Tretiakov, D. Clarke, G.-W. Chern, Y. B. Bazaliy, and O. Tchernyshyov, Dynamics of Domain Walls in Magnetic Nanostrips, *Phys. Rev. Lett.* **100**, 127204 (2008).
- [46] K. A. van Hoogdalem, Y. Tserkovnyak, and D. Loss, Magnetic texture-induced thermal Hall effects, *Phys. Rev. B* **87**, 024402 (2013).
- [47] S. K. Kim, K. Nakata, D. Loss, and Y. Tserkovnyak, Tunable Magnonic Thermal Hall Effect in Skyrmion Crystal Phases of Ferrimagnets, *Phys. Rev. Lett.* **122**, 057204 (2019).
- [48] J. Lan, W. Yu, and J. Xiao, Geometric magnonics with chiral magnetic domain walls, *Phys. Rev. B* **103**, 214407 (2021).
- [49] H. Yang, J. Liang, and Q. Cui, First-principles calculations for Dzyaloshinskii-Moriya interaction, *Nat. Rev. Phys.* **5**, 43 (2022).
- [50] J.-H. Moon, S.-M. Seo, K.-J. Lee, K.-W. Kim, J. Ryu, H.-W. Lee, R. D. McMichael, and M. D. Stiles, Spin-wave propagation in the presence of interfacial Dzyaloshinskii-Moriya interaction, *Phys. Rev. B* **88**, 184404 (2013).
- [51] D. Cortés-Ortuño and P. Landeros, Influence of the Dzyaloshinskii-Moriya interaction on the spin-wave spectra of thin films, *J. Phys.: Condens. Matter* **25**, 156001 (2013).
- [52] W. Yu, Micromagnetic simulation with COMSOL Multiphysics, 2021 (unpublished).
- [53] H. Wu and J. Lan, Curvilinear manipulation of polarized spin waves, *Phys. Rev. B* **105**, 174427 (2022).
- [54] J. Zou, S. K. Kim, and Y. Tserkovnyak, Tuning entanglement by squeezing magnons in anisotropic magnets, *Phys. Rev. B* **101**, 014416 (2020).
- [55] J. Lan, W. Yu, and J. Xiao, Antiferromagnetic domain wall as spin wave polarizer and retarder, *Nat. Commun.* **8**, 178 (2017).
- [56] Y. Liu, Z. Xu, L. Liu, K. Zhang, Y. Meng, Y. Sun, P. Gao, H.-W. Zhao, Q. Niu, and J. Li, Switching magnon chirality in artificial ferrimagnet, *Nat. Commun.* **13**, 1264 (2022).
- [57] S. Datta, *Electronic Transport in Mesoscopic Systems* (Cambridge University Press, Cambridge, 1995).